The effect of the exchange-correlation functional on H2 dissociation on Ru(0001)

M. Wijzenbroek and G. J. Kroes

Citation: The Journal of Chemical Physics **140**, 084702 (2014); doi: 10.1063/1.4865946
View online: http://dx.doi.org/10.1063/1.4865946
View Table of Contents: http://scitation.aip.org/content/aip/journal/jcp/140/8?ver=pdfcov
Published by the AIP Publishing

The effect of the exchange-correlation functional on H_2 dissociation on Ru(0001)

M. Wijzenbroek and G. J. Kroes
Leiden Institute of Chemistry, Gorlaeus Laboratories, Leiden University, P.O. Box 9502, 2300 RA, Leiden, The Netherlands

(Received 25 November 2013; accepted 4 February 2014; published online 25 February 2014)

The specific reaction parameter (SRP) approach to density functional theory (DFT) has enabled a chemically accurate description of reactive scattering experiments for activated H_2–metal systems (H_2 + Cu(111) and Cu(100)), but its application has not yet resulted in a similarly accurate description of non-activated or weakly activated H_2-metal systems. In this study, the effect of the choice of the exchange-correlation functional in DFT on the potential energy surface and dynamics of H_2 dissociation on Ru(0001), a weakly activated system, is investigated. In total, full potential energy surfaces were calculated for over 20 different functionals. The functionals investigated include functionals incorporating an approximate description of the van der Waals dispersion in the correlation functional (vdW-DF and vdW-DF2 functionals), as well as the revTPSS meta-GGA. With two of the functionals investigated here, which include vdW-DF and vdW-DF2 correlation, it has been possible to accurately reproduce molecular beam experiments on sticking of H_2 and D_2, as these functionals yield a reaction probability curve with an appropriate energy width. Diffraction probabilities computed with these two functionals are however too high compared to experimental diffraction probabilities, which are extrapolated from surface temperatures (T_s) $\geq$ 500 K to 0 K using a Debye–Waller model. Further research is needed to establish whether this constitutes a failure of the two candidate SRP functionals or a failure of the Debye–Waller model, the use of which can perhaps in future be avoided by performing calculations that include the effect of surface atom displacement or motion, and thereby of the experimental T_s. © *2014 AIP Publishing LLC*. [http://dx.doi.org/10.1063/1.4865946]

I. INTRODUCTION

To perform accurate dynamics calculations on molecule–surface reactions, such as the dissociation of small molecules on metal surfaces, accurate potential energy surfaces (PESs) are needed. Due to the large, delocalized nature of these systems, electronic structure calculations on such systems are computationally expensive. Efficient electronic structure methods are therefore needed if one wishes to study such a system in detail.

For molecule–surface reactions, one is limited to an electronic structure method with a favourable computational scaling, which in practice means density functional theory (DFT)[1,2] using an approximate exchange-correlation (XC) functional on the generalized gradient approximation (GGA)[3,4] level. As of yet, it is not quantitatively known how large the error of using such an approximate XC functional is for barrier heights of molecule–surface reactions. Such studies have been performed for gas-phase reactions,[5,6] but remain challenging for molecule–surface reactions because of the lack of benchmark databases available for these systems. For chemisorption energies a database of experimental values is available,[7] but for barrier heights no such databases exist. Perhaps the closest one can get to such a database is a recently started database of molecule–surface barrier heights.[8,9] This database, however, is based on DFT calculations using the RPBE[10] functional, and can as such not be used to estimate the error made by the use of DFT in general.

For molecule–surface interactions, additional complications arise because also the surface introduces many additional degrees of freedom: energy exchange is possible with surface phonons and electron-hole pair excitations are possible.[11–13] For H_2 dissociation on metal surfaces, these effects can however be mostly avoided. Energy exchange with surface phonons may be expected to be a small effect[14] due to the large mass mismatch between the H_2 molecule and a surface atom. It has furthermore been argued that electron-hole pair excitation should only have a small effect on H_2–surface reactions.[15] These effects are discussed further in Sec. II A.

For dissociation of H_2 on Cu(111), an activated late barrier molecule–surface reaction, it has been shown that neither of two popular XC functionals in the surface science community, the PW91[16] and the RPBE[10] functionals, could give a good agreement with experiment.[17,18] By employing a "specific reaction parameter" (SRP)[19] approach adapted to molecule–surface reactions,[17,18] a good agreement could be obtained with a broad range of reaction and scattering experiments. The functional that was obtained as a result of the SRP procedure for H_2 on Cu(111) was also found to work well for H_2 on Cu(100).[20] In the SRP procedure previously used for H_2 on Cu(111), a parameter (α) mixing two functionals by

$$E_{\mathrm{SRP}} = \alpha \cdot E_a + (1-\alpha) \cdot E_b, \tag{1}$$

where E_a and E_b are the XC energies obtained from the two functionals, was fitted in such a way that the reaction

probability obtained from the SRP (mixed) functional matched the values measured in molecular beam experiments. As a result of this fitting procedure, the functional provides a reasonable description of the barrier height for reaction.[17] The test of a SRP functional is that it should also yield a good description of other observables than the one it was fitted to for the system investigated. It should be pointed out however that it is possible that one particular functional can already yield a good description of the ongoing processes, and as such the mixing procedure may not be needed.

It is currently not clear to what extent such a procedure is valid for weakly activated early barrier molecule–surface reactions. H_2 dissociation on Ru(0001) is an example of such an early barrier molecule–surface reaction. This reaction is also of catalytic importance, as ruthenium-based catalysts can be used to catalyse the production of ammonia from H_2 and N_2,[21–25] and the dissociation of H_2 on ruthenium is one of the elementary steps in this process. Although the dissociation of N_2 on ruthenium is thought to be the rate determining step in this process,[26,27] it is nonetheless important to have a detailed understanding of the other steps.

Previously, PESs were constructed for H_2 dissociation on Ru(0001),[28] and quantum dynamics calculations have been performed[29,30] to compare two DFT XC functionals, PW91[16] and RPBE,[10] with each other. Comparisons have also been made to experimental molecular beam studies on dissociative adsorption[31] as well as diffractive scattering.[30] The results of the comparison with experiments showed that neither functional could properly describe reaction over the entire interval of incidence energy, in the sense that the calculated reaction probability curve as a function of incidence energy was too narrow compared to the experimental curve, suggesting the energetic corrugation of the used potential energy surfaces to be too small.[30,31] The same semi-empirical mixture of these two functionals as the one which worked well for H_2 dissociation on Cu(111)[17,18] was also not able to describe the reaction probability of H_2 on Ru(0001) over the entire range of incidence energies. Additionally, calculated diffraction probabilities were generally (somewhat) higher than the experimental diffraction probabilities. This discrepancy was attributed to the used XC functionals.[30] It was argued that the van der Waals interaction, which is not taken into account in the usual (semi-)local XC functionals,[32,33] could be important for an early barrier system such as H_2 dissociation on Ru(0001). To our knowledge, so far no studies exist in which the van der Waals interaction has been taken into account explicitly in dynamics calculations on H_2 dissociation on metal surfaces. Furthermore, in calculations on H_2 on Ru(0001) in which electron-hole pair excitations were incorporated by the use of electronic friction coefficients, the width of the reaction probability curve was found to be influenced only weakly by electronic friction.[34]

In the present work, an extensive study of XC functionals for H_2 dissociation on Ru(0001) is reported. The goal of the present work is twofold: first, to determine whether improved XC functionals, such as van der Waals-corrected functionals or meta-GGA functionals, can lead to an improved description of this system, and second, to obtain a SRP functional which is able to describe this system. To achieve this, potential energy surfaces were constructed for H_2 on Ru(0001) using more than 20 different XC functionals. Barrier heights for reaction are analysed and from this analysis, and based on reaction probabilities obtained from quasi-classical dynamics calculations, interesting functionals are identified. Quantum dynamics calculations are performed for the functionals giving the best description of reaction to compare with diffraction experiments.

In Sec. II, the methods used are explained, starting with the dynamical model and dynamics methods in Sec. II A. The construction of potential energy surfaces is discussed in Sec. II B. Section II C focuses on the calculation of observables. In Sec. II D, the computational details are given. In Sec. III, the results of the calculations are shown and discussed, starting with an overview of the constructed potential energy surfaces in Sec. III A. State-resolved reaction probabilities and rotational quadrupole alignment parameters are discussed in Sec. III B and simulations of molecular beam sticking experiments are discussed in Sec. III C. Diffractive scattering and reaction at off-normal incidence are discussed in Sec. III D. Finally, in Sec. IV, the conclusions are given.

II. THEORY

A. Dynamical model

Both quantum dynamics and quasi-classical dynamics calculations have been performed. For all calculations, the Born-Oppenheimer Static Surface (BOSS) model is used. In the BOSS model, two approximations are made. First of all, the Born-Oppenheimer approximation[35] is made. Second, a static surface approximation is made, in which the surface atoms are assumed to be fixed at their ideal lattice positions, and therefore, only the 6 degrees of freedom of the H_2 molecule are taken into account in the dynamics. The coordinate system used is shown in Figure 1(a).

The use of these approximations for H_2/metal surface scattering is supported by previous work. For H_2 dissociation on Pt(111) it has previously been argued that nonadiabatic effects should not play an important role, for

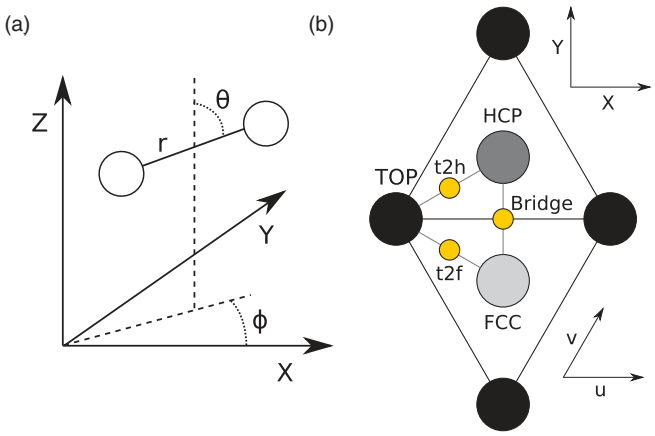

FIG. 1. (a) The center of mass coordinate system used for the description of the H_2 molecule. (b) The surface unit cell and the sites considered. The origin of the coordinate system ($X = u = 0$, $Y = v = 0$, $Z = 0$) is at a top layer atom (top site).

reasons that are generic to H_2/metal systems.[15] Non-adiabatic effects have been incorporated in calculations on H_2 dissociation on Cu(111),[36,37] Cu(110),[38] and Ru(0001),[34] using electronic friction. No large non-adiabatic effects were found in these dynamics calculations, suggesting that the Born-Oppenheimer approximation works well for these systems.

The validity of the static surface approximation has been tested recently for H_2 dissociation on Cu(111) using *ab initio* molecular dynamics (AIMD) calculations,[39] in which surface atoms in 3 layers of a 2×2 unit cell were allowed to move, and static corrugation model (SCM) calculations,[40] which excluded energy exchange with the surface but included the displacement of surface atoms and surface expansion effects. In these studies, good agreement was found between static surface calculations and calculations at the experimental surface temperature ($T_s = 120$ K). These calculations suggested thermal expansion of the surface to be important, which has been tested recently.[41]

For H_2 dissociation on Ru(0001), the neglect of surface temperature is not expected to have a big effect. The importance of energy exchange is not expected to be large. Due to the large mass mismatch between a H_2 molecule and a surface atom, motion of the H_2 molecule and the surface atoms should only be weakly coupled, i.e., the effect of energy exchange should be small. The effect of the static displacement of surface atoms is also expected to be small. This is because H_2 dissociation on Ru(0001) is an early barrier system: the barriers are located far from the surface, therefore the coupling between the H_2 molecule located at the barrier and the closest surface atoms should be small. Finally, also thermal expansion is expected to be a rather small effect. Bulk ruthenium expands by about 0.24% in a and 0.36% in c from 0 K to 500 K.[42] The first interlayer spacing d_{12} contracts slightly with increasing surface temperature.[43] It should be noted that the surface temperature used in the diffraction experiments ($T_s = 500$ K[30]) is somewhat higher than the surface temperature used in the molecular beam experiments ($T_s = 180$ K[31]), which suggests that if surface temperature does play a role it would do so predominantly in the diffraction experiments.

1. Quantum dynamics

For the quantum dynamics calculations, a time-dependent wave packet (TDWP)[44,45] method was used. To represent the wave packet in Z, r, X, and Y, a discrete variable representation (DVR)[46] was used, and to represent the wave packet in the angular degrees of freedom, a finite base representation (FBR)[47,48] was used. To transform the wave function from the FBR space to the DVR space, and vice versa, Fast Fourier transforms[49] and discrete associated Gauss–Legendre transforms[47,48] were used. To propagate the wave packet according to the time dependent Schrödinger equation, the split operator method[50] is used. The initial wave packet is placed far away from the surface, where only a negligibly small interaction is present, and is written as a product of a Gaussian wave packet for motion perpendicular to the surface, plane waves for motion parallel to the surface and a rovibrational wavefunction describing the initial state of the molecule.[45] The reflected wave packet is analysed using the scattering amplitude formalism[51–53] at $Z = Z_\infty$, yielding S-matrix elements for state-to-state scattering. For large r or Z, optical potentials[54] are used to absorb the reacted (r) or analysed (Z) wave packet. Scattering probabilities were obtained from S-matrix elements over the entire range of energies present in the wave packet. The fully initial state-resolved reaction probability is defined as

$$P_r(v, J, m_J) = 1 - \sum_{\substack{v', J', m'_J, \\ n, m}} P_{scat}(v, J, m_J \rightarrow v', J', m'_J, n, m), \quad (2)$$

where $P_{scat}(v, J, m_J \rightarrow v', J', m'_J, n, m)$ are the state to state scattering probabilities, v (v'), J (J'), m_J (m'_J) the initial (final) vibrational, rotational, and magnetic rotational quantum numbers, respectively, and n and m the quantum numbers for diffraction.

2. Quasi-classical dynamics

In the quasi-classical dynamics[55] calculations, the Hamilton equations of motion were integrated with the predictor-corrector method of Bulirsch and Stoer.[56] The initial conditions of the H_2 molecules are selected using standard Monte Carlo methods. To obtain m_J resolved reaction probabilities, the initial angular momentum of the molecule is fixed by $L = \sqrt{J(J+1)}\hbar$ and its orientation is chosen randomly with the constraint $\cos \vartheta_L = m_J/\sqrt{J(J+1)}$, where ϑ_L is the angle between the angular momentum vector and the surface normal. At each point on a reaction probability curve, to get accurate results, at least 10^4 trajectories were computed. The H_2 molecule was initially placed at $Z = 9$ Å. The molecule was considered to have dissociated when $r > 2.25$ Å.

B. Construction of potential energy surfaces

Full six-dimensional (6D) PESs were constructed from self-consistent DFT calculations with various XC functionals. To construct a PES, a number of DFT calculations are performed. First, to obtain the lattice constants a and c to use for ruthenium, a bulk HCP unit cell containing two atoms was set up. This unit cell was relaxed, during which the size and shape of the unit cell was allowed to change. Second, to obtain the structure of the slab to use, a slab was set up with a structure resembling the bulk structure obtained in the first step, after which the positions of the atoms were allowed to relax in the direction perpendicular to the slab. Finally, to map out the molecule–surface interaction on various sites in the Ru(0001) surface unit cell, a H_2 molecule was added to the unit cell obtained in the second step, and a large number of single point calculations were carried out with the H_2 molecule in various geometries.

To interpolate the results from the single point calculations, the corrugation reducing procedure (CRP) was

used.[57,58] In the CRP, the PES is written as

$$V^{6D}(\vec{r}) = I^{6D}(\vec{r}) + \sum_{i}^{2} V_i^{3D}(\vec{r}_i), \quad (3)$$

in which V^{6D} is the full 6D PES of the H_2/surface system, $\vec{r}$ is a vector representing the coordinates of the H_2 molecule with respect to the surface, I^{6D} is the so-called 6D interpolation function of the H_2/surface system, V_i^{3D} is the three-dimensional (3D) PES of the H/surface system, and $\vec{r}_i$ is a vector representing the coordinates of the ith H atom with respect to the surface. To interpolate the 3D PES of the H/surface system the CRP is applied again using

$$V_i^{3D}(\vec{r}_i) = I_i^{3D}(\vec{r}_i) + \sum_{j}^{N} V^{1D}(R_{ij}), \quad (4)$$

in which I_i^{3D} is the 3D interpolation function describing the H/surface system, N is the number of surface atoms to take into account in the summation, V^{1D} is a one-dimensional (1D) function mimicking the interaction of a hydrogen atom and a single surface atom and R_{ij} is the distance between the hydrogen atom i and surface atom j. It should be noted at this point that a good V^{1D} function reduces the corrugation in I^{3D}, but the choice of this function is somewhat arbitrary.[57]

In the interpolation a 60° skewed coordinate system (u, v) is used (see also Figure 1(b)). In the discussion below this (u, v) coordinate system is assumed to be scaled such that the closest surface atom-surface atom distance within a layer is unity. The CRP allows for a much smoother interpolation of the PES than a direct interpolation, because the 6D interpolation function I^{6D} is much less corrugated in the u, v, θ, and ϕ degrees of freedom than V^{6D}.[57]

For the interpolation of I^{6D}, a total of 29 configurations (u, v, θ, ϕ) are used, spread over 6 different sites (u, v) (see also Figure 1(b)). The used configurations have been listed in Table I. The interpolation is done in several steps, similar to the method used for H_2/Cu(100) by Olsen *et al.*[58] First, for every configuration, the interpolation over the r and Z degrees of freedom is performed. This interpolation is performed over a 14×15 ($r \times Z$) grid using a two-dimensional (2D) cubic spline interpolation. Then, on every site, the interpolation is performed over the θ and ϕ degrees of freedom using symmetry adapted sine and cosine functions. Finally, the interpolation over u and v is performed, again using symmetry adapted sine and cosine functions.

TABLE I. Configurations used in the interpolation of H_2/Ru(0001) PES. The sites listed here correspond to the sites listed in Table II, and are also shown graphically in Figure 1.

Site	θ	ϕ
Top	0	
Top	90	0, 30
t2h	0	
t2h	45	30, 120, 210
t2h	90	30, 120
HCP	0	
HCP	45	30, 210
HCP	90	0, 30
Bridge	0	
Bridge	90	0, 60, 90
FCC	0	
FCC	45	150, 330
FCC	90	0, 330
t2f	0	
t2f	45	150, 240, 330
t2f	90	240, 330

TABLE II. Sites used in the interpolation of the H/Ru(0001) PES.

Site	u	v
Top	0	0
Bridge	1/2	0
HCP	1/3	1/3
t2h	1/6	1/6
ϵ	1/3	1/6
τ	1/6	0
η	1/3	0
t2f	1/3	−1/6
ϵ'	1/2	−1/6
FCC	2/3	−1/3

For the interpolation of I^{3D}, a total of 10 sites in (u, v) are used. The used configurations have been listed in Table II. The interpolation is performed in two steps. First, for every site, a 1D cubic spline interpolation over 57 points in Z is performed. Then the interpolation over the u and v degrees of freedom is performed, using symmetry adapted sine and cosine functions. For V^{1D}, the spline interpolation of the interaction of the H atom above the top site is used, similar to previous studies.[57]

From $Z = 3.4$ Å to $Z = 4$ Å, the PES is switched from the full V^{6D} to a 2D gas phase interaction V^{2D}, as the dependence on the other degrees of freedom far away from the surface is small. This gas phase potential is given by

$$V^{2D}(r, Z) = V^{ext}(Z) + V^{gas}(r), \quad (5)$$

where V^{ext} is a function describing the dependence of the PES on Z beyond $Z = 4$ Å and V^{gas} is the interaction at $Z = Z_{max}$. In the present work, these functions are represented by 1D cubic splines, with Z_{max} taken to be 6 Å.

C. Calculation of observables

1. Initial state-resolved reaction probability

Degeneracy averaged reaction probabilities P_{deg} were computed by

$$P_{deg}(v, J) = \sum_{m_J=0}^{J} \left(2 - \delta_{m_J 0}\right) P_r(v, J, m_J)/(2J + 1), \quad (6)$$

in which P_r is the fully initial state-resolved reaction probability, δ is the Kronecker delta, and v, J, and m_J are the initial vibrational, rotational, and magnetic rotational quantum numbers of H_2, respectively.

2. Rotational quadrupole alignment

The rotational quadrupole alignment parameter is a measure of the dependence of the reaction on the orientation of the molecule with respect to the surface. It can be written as

$$A_0^{(2)} = \langle 3\cos^2\vartheta_L - 1\rangle, \tag{7}$$

in which ϑ_L is the angle between the angular momentum vector and the surface normal. It can also be computed as[59]

$$A_0^{(2)}(v, J) = \frac{\sum_{m_J} P_r(v, J, m_J)\left(\frac{3m_J^2}{J(J+1)} - 1\right)}{\sum_{m_J} P_r(v, J, m_J)}. \tag{8}$$

3. Molecular beams

Molecular beams used in experiments do generally not consist of molecules in a single state with one particular incidence energy. To compare with the molecular beams used in experiments,[31] two things have to be taken into account. First, the state-resolved reaction probabilities should be averaged over the rovibrational states populated in the molecular beam. Second, the experimental spread of incidence energies should be taken into account. The first point is addressed by

$$R_{\text{mono}}(E_i; T_n) = \sum_{v,J} F_B(v, J; T_n) P_{\text{deg}}(E_i, v, J), \tag{9}$$

in which R_{mono} is the mono-energetic reaction probability averaged over all states present in the molecular beam with a nozzle temperature T_n. The reaction probability of each state is weighed with the Boltzmann factor

$$F_B(v, J; T_n) = \frac{w(J)F(v, J; T_n)}{\sum_{v', J' \equiv J \pmod 2} F(v', J'; T_n)} \tag{10}$$

with

$$F(v, J; T_n) = (2J+1)\exp\left(-E_{\text{vib}}(v, J)/(k_B T_n)\right) \cdot \exp\left(-E_{\text{rot}}(v, J)/(0.8 \cdot k_B T_n)\right). \tag{11}$$

In Eq. (10), the summation runs only over the values of J' which have the same parity as J. k_B is the Boltzmann constant and E_{vib} and E_{rot} are the vibrational and rotational energy, respectively, of the (v, J) state. In these equations, it is assumed that the rotational temperature of the molecules in the beam is lower than the nozzle temperature ($T_{\text{rot}} = 0.8 \cdot T_n$).[60] In the research reported below it is also assumed that the ratio of ortho- and para-H_2 or D_2 is equivalent to the high temperature limit, given by $w(J)$, which is the case in experiments, as the gas cylinder is stored at room temperature and conversion of ortho- and para-hydrogen does not happen on the time scale of the experiment. For H_2, $w(J)$ is equal to 1/4 for even J and 3/4 for odd J. For D_2 it is equal to 2/3 for even J and 1/3 for odd J.

The mono-energetic reaction probability then has to be averaged over the translational energy distribution by[18]

$$R_{\text{beam}} = \frac{\int_0^\infty f(v_i; T_n) R_{\text{mono}}(E_i; T_n) \mathrm{d}v_i}{\int_0^\infty f(v_i; T_n)\mathrm{d}v_i}. \tag{12}$$

TABLE III. Parameters used for the molecular beam simulations of H_2 and D_2 on Ru(0001). The parameters were obtained from fits of Eq. (14) to the experimental time of flight spectra.[63]

	$\langle E_i\rangle$ (eV)	v_0 (m/s)	α (m/s)	T_{nozzle} (K)
	0.061	2375.3	167.3	300
	0.075	2641.8	329.2	300
	0.129	3334.2	607.5	500
	0.182	3862.9	852.0	700
H_2	0.232	4264.6	1088.9	900
	0.274	4564.2	1266.7	1100
	0.328	4907.6	1473.7	1300
	0.377	5154.2	1687.5	1500
	0.430	5391.6	1901.9	1700
	0.078	1932.3	193.6	300
	0.124	2372.5	295.1	500
	0.219	3090.8	527.4	900
D_2	0.316	3625.4	765.6	1300
	0.363	3818.9	908.9	1700
	0.455	4051.2	1261.8	1700
	0.466	4268.9	1097.1	1700

Here f is the flux weighted velocity distribution, which is given by[61,62]

$$f(v_i; T_n)\mathrm{d}v_i = C v_i^3 \exp[-(v_i - v_0)^2/\alpha^2]\mathrm{d}v_i. \tag{13}$$

In this equation C is a constant, v_i is the velocity of the molecule, v_0 is the stream velocity, and α is a parameter describing the width of the velocity distribution. The parameters for the H_2 and D_2 beams of Groot *et al.*[31] are shown in Table III. These parameters were obtained by fitting

$$G(t; T_n) = c_1 + c_2 v^4 \exp[-(v_i - v_0)^2/\alpha^2] \tag{14}$$

to the experimental time of flight spectra.[63] It is noted here that the parameters describing the H_2 molecular beam differ somewhat from the parameters presented earlier,[30] as an error was made in the analysis of the TOF measurements.[63]

4. Diffraction probabilities

To compare with the experimental diffraction probabilities,[30] first rovibrationally elastic diffraction probabilities were computed by

$$P_{nm}(v, J, m_J) = \sum_{m_J''=0}^{J} ((2 - \delta_{m_J'' 0}) \cdot P_{\text{scat}}(v, J, m_J \to v' = v, J' = J, m_J'', n, m)), \tag{15}$$

where P_{nm} is the rovibrationally elastic probability for scattering into the diffraction state denoted by the n and m quantum numbers. These probabilities are then degeneracy averaged by

$$P_{nm}(v, J) = \sum_{m_J=0}^{J} (2 - \delta_{m_J 0}) P_{nm}(v, J, m_J)/(2J+1). \tag{16}$$

Because in experiments mostly $J = 0$ and $J = 1$ H_2 were present with a narrow energy distribution,[30,64] in particular

TABLE IV. The exchange-correlation functionals used in this work. Also shown are the lattice constants obtained for ruthenium (best matches shown in bold typeface).

Name	Type	Exchange	Correlation	a (Å)	c (Å)
BLYP	GGA	Becke88[4]	LYP[65]	2.775	4.363
BP	GGA	Becke88[4]	Perdew86[66]	2.735	4.308
HTBS	GGA	HTBS[67]	PBE[68]	**2.706**	**4.268**
PBEα	GGA	PBEα=0.5[69]	PBE[68]	2.720	4.288
PBEαLDA	GGA	PBEα=0.5[69]	LDA (PW[70])	2.778	4.369
PBEαLYP	GGA	PBEα=0.5[69]	LYP[65]	2.763	4.348
PBEα:RPBE(85:15)LYP	GGA	0.85 PBEα=0.5[69] + 0.15 RPBE[10]	LYP[65]	2.767	4.353
PBE	GGA	PBE[68]	PBE[68]	2.730	4.304
PBELDA	GGA	PBE[68]	LDA (PW[70])	2.790	4.387
PBELYP	GGA	PBE[68]	LYP[65]	2.775	4.365
PBEP	GGA	PBE[68]	Perdew86[66]	2.735	4.310
PBE-vdW-DF	vdW-DF	PBE[68]	vdW-DF[71]	2.751	4.336
PBE-vdW-DF2	vdW-DF	PBE[68]	vdW-DF2[72]	2.754	4.341
PBE:RPBE(50:50)-vdW-DF	vdW-DF	0.5 PBE[68] + 0.5 RPBE[10]	vdW-DF[71]	2.758	4.347
PW91	GGA	PW91[16]	PW91[16]	2.732	4.305
(revPBE-)vdW-DF	vdW-DF	revPBE[73]	vdW-DF[71]	2.761	4.351
revTPSS	Meta-GGA	revTPSS[74]	revTPSS[74]	**2.690**	**4.246**
RPBE	GGA	RPBE[10]	PBE[68]	2.744	4.325
RPBELYP	GGA	RPBE[10]	LYP[65]	2.790	4.388
RPBE-vdW-DF	vdW-DF	RPBE[10]	vdW-DF[71]	2.765	4.357
RPBE-vdW-DF2	vdW-DF	RPBE[10]	vdW-DF2[72]	2.768	4.362
(rPW86-)vdW-DF2	vdW-DF	rPW86[72]	vdW-DF2[72]	2.799	4.412
WC	GGA	WC[75]	PBE[68]	**2.706**	**4.267**
Experiment (295 K)[76]				2.706	4.281
Extrapolation (0 K)[42]				2.703	4.274

at the lowest incidence energies, a reasonable approximation should be the use of a beam of cold n-H_2 (25% $J = 0$, 75% $J = 1$) with a monochromatic energy. In the calculations performed here this approximation is made.

D. Computational details

For the electronic structure calculations VASP[77–79] (version 5.2.12) was used. To allow the use of XC functionals not present in VASP, the LibXC[80] library (version 1.2.0) has been used.

Potential energy surfaces have been constructed for a wide range of XC functionals. The functionals used are listed in Table IV. For the GGA functionals, except for the PBELDA and PBEαLDA functionals, the standard[81] VASP ultrasoft pseudopotentials[82] were used. For all other functionals, PAW[83] potentials[84] were used. The vdW-DF functionals were evaluated within the scheme of Román-Pérez and Soler.[85]

Tests were performed on the bulk system and the molecule–surface system to find a k-point sampling and plane wave cutoff yielding converged results. The convergence was found to be nearly independent of the XC functional, although for vdW-DF functionals the convergence was somewhat less good, but still good enough. For this reason, as well as consistency, the k-point sampling and plane wave cutoff were chosen to be equal for all functionals. For the bulk calculations, a 20×20×20 Γ-centered Monkhorst-Pack grid was used with a plane wave cutoff of 450 eV. For the slab calculations, a 20×20×1 Γ-centered Monkhorst-Pack grid was used with the same plane wave cutoff. For the single point calculations to determine the molecule–surface interaction, a 8×8×1 Γ-centered Monkhorst-Pack grid was used with a plane wave cutoff of 350 eV. A 2×2 supercell with a vacuum of 13 Å between images of the slab was used. For all calculations, to speed up convergence, Fermi smearing was used with a width of 0.1 eV. Finally, in all calculations a five-layer slab was considered. Convergence tests with respect to the number of layers for two geometries close to the transition state for the top($\theta = 90°$, $\phi = 0°$) and hcp($\theta = 90°$, $\phi = 30°$) configurations, showed that for a range of GGA functionals the difference between using a five- and seven-layer slab was on average about 5 meV for the top to bridge case and about 10 meV for the hcp case. This error was found to not depend much on the chosen XC functional.

For the quantum dynamics calculations on reaction at normal incidence, two wave packets with different energy ranges were propagated. The lower energy range was taken from 40 meV to 200 meV, the high energy range from 150 meV to 600 meV. For calculations on diffraction at off-normal incidence however, only the lower energy range was calculated. Convergence tests indicated that the same parameters could be used for all calculations. The parameters used are shown in Table V.

III. RESULTS AND DISCUSSION

A. Potential energy surfaces

It should be clear that with the large number of PESs considered here, a full analysis is beyond the scope of this

TABLE V. Parameters for quantum dynamics calculations on H_2 dissociation and scattering from Ru(0001). Values for odd values of J, where different, are listed in parentheses. All values are in atomic units.

Parameter	Description	Value
$N_X = N_Y$	Number of grid points in X and Y	18
$J_{\max}$	Maximum J in basis set	16(17)
$m_{J,\max}$	Maximum m_J in basis set	16(17)
$r_{\min}$	Start of grid in r	0.4
Δr	Spacing of grid in r	0.25
N_r	Number of grid points in r	32
$Z_{\min}$	Start of grid in Z	−1.0
ΔZ	Spacing of grid in Z	0.135
N_Z	Number of grid points in Z	128
$N_{Z,\mathrm{sp}}$	Number of grid points in specular Z	256
Δt	Propagation time step	5.0
Δt_{ana}	Analysis time step	40.0
Z_0	Center of initial wave packet	16.955
Z_∞	Location of analysis line	12.5
A_2^Z	Optical potential strength in Z	0.002
$Z_{\min}^{\mathrm{opt}}$	Start optical potential in Z	12.5
$Z_{\max}^{\mathrm{opt}}$	End optical potential in Z	16.145
$A_2^{Z,\mathrm{sp}}$	Optical potential strength in Z_{sp}	0.0035
$Z_{\mathrm{sp,min}}^{\mathrm{opt}}$	Start optical potential in Z_{sp}	22.355
$Z_{\mathrm{sp,max}}^{\mathrm{opt}}$	End optical potential in Z_{sp}	33.425
A_2^r	Optical potential strength in r	0.008
$r_{\min}^{\mathrm{opt}}$	Start optical potential in r	4.15
$r_{\max}^{\mathrm{opt}}$	End optical potential in r	8.15

paper. It is nonetheless important, however, to highlight several features of the created PESs, thereby extending the previous analysis by Luppi *et al.*[28]

Contour plots of all 2D cuts that were used for the construction of the PES were made and the transition states on these contour plots were identified. In Figure 2, contour plots of several high symmetry configurations are shown, from one of the PESs which was found to give the best description of the molecular beam experiments (see also Sec. III C). Consistent with previous calculations,[28] the barrier height increases in the order top < t2h/t2f < bridge < hcp/fcc. In most cases, except for the rPW86-vdW-DF2 functional, the hcp barrier was found to be slightly higher (up to 46 meV for the revTPSS functional) than the fcc barrier. It should be emphasized that most of the trends seen in Figure 2 are qualitatively reproduced by most functionals, but quantitatively (large) differences can be found.

A notable feature of the H_2 on Ru(0001) PES is the presence of two transition states on several 2D cuts. On the top site two transition states are found with a well in between. This feature is general for all functionals. This is also, for several functionals, found to be the case for the t2h($\theta = 90^\circ$, $\phi = 120^\circ$) and t2f($\theta = 90^\circ$, $\phi = 240^\circ$) configurations. Differences were found with respect to the relative energy of the early and late transition states present in 2D cuts above the top site. For most exchange-correlation functionals, the early transition state was found to be highest in energy, but for several others the late transition state was found to be highest in energy. The difference between the two transition state energies ($E_{\mathrm{top}}^{\mathrm{late}} - E_{\mathrm{top}}^{\mathrm{early}}$) was found to vary between −0.64 eV

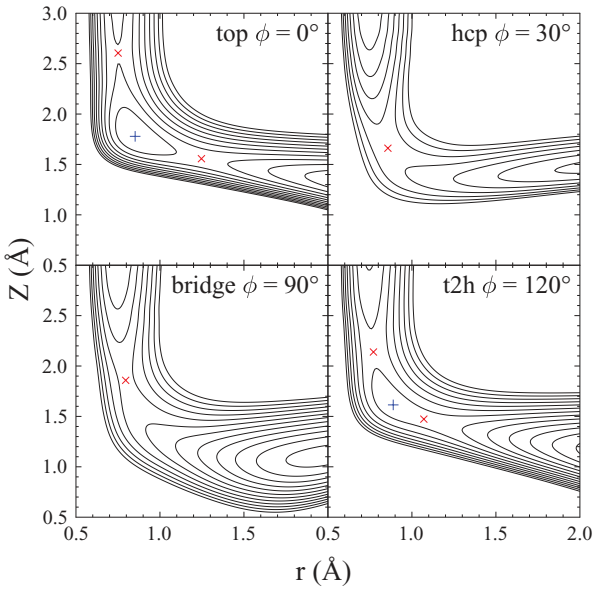

FIG. 2. Contour plots of the H_2 on Ru(0001) PES for four high symmetry configurations with $\theta = 90^\circ$, for the PBE-vdW-DF2 functional. Transition states are indicated by (red) crosses, while local minima in the potential are indicated by (blue) plus symbols. The spacing between contour lines is 0.1 eV.

for the WC functional to 0.14 for the rPW86-vdW-DF2 functional. These results suggest that care should be taken with the choice of an exchange-correlation functional, as this could have a drastic influence on the dynamics. Transition state geometries and energies for the geometries depicted in Figure 2 are given in Table VI, for the PBE-vdW-DF2, PBE:RPBE(50:50)-vdW-DF, and PBE functionals. The two vdW-DF functionals, included because they yield the best description of the molecular beam experiments (see Sec. III C), yield similar transition state geometries and energies, and in all cases transition states which are closer to the surface than obtained with the reference PBE functional.

The energetic corrugation has also been considered. The energetic corrugation is defined here as the difference between the hcp($\theta = 90^\circ$, $\phi = 30^\circ$) transition state energy and the top($\theta = 90^\circ$, $\phi = 0^\circ$) transition state energy. The energetic corrugation of a PES is a useful quantity as it is typically found to correspond to the "width" of the reaction probability curve for activated dissociation systems.[86] By the width, one usually means the range of energies over which the reaction probability increases more or less linearly from an onset energy that is close to the reaction threshold to an energy at which the reaction probability starts to plateau. As such, the width of the reaction probability curve is inversely related to the slope of the reaction probability over this energy region, and the slope of the curve is therefore also related to the energetic corrugation of the PES. In this paper, the width of the reaction probability curve is rather loosely defined in this way. In some cases reaction probability curves may be fitted rather well with sigmoidal functions like

$$S(E) = \frac{A}{2}\left[1 + \mathrm{erf}\left(\frac{E - E_0}{W}\right)\right], \qquad (17)$$

TABLE VI. Transition state geometries and transition state energies, relative to the gas phase minimum, for the four geometries depicted in Figure 2. Where available, both transition states have been indicated. With MIX-vdW-DF the PBE:RPBE(50:50)-vdW-DF functional is meant.

Parameter	Top 1	Top 2	t2h 1	t2h 2	bri	hcp
ϕ	0°	0°	120°	120°	90°	30°
$Z_{\text{PBE-vdW-DF2}}$ (Å)	2.605	1.557	2.139	1.473	1.858	1.661
$Z_{\text{MIX-vdW-DF}}$ (Å)	2.605	1.559	2.122	1.474	1.830	1.646
Z_{PBE} (Å)	2.736	1.544	2.350	...	2.069	1.926
$r_{\text{PBE-vdW-DF2}}$ (Å)	0.751	1.247	0.771	1.071	0.796	0.857
$r_{\text{MIX-vdW-DF}}$ (Å)	0.751	1.249	0.771	1.072	0.799	0.861
r_{PBE} (Å)	0.757	1.251	0.767	...	0.785	0.805
$E_{\text{PBE-vdW-DF2}}$ (eV)	0.004	−0.073	0.115	0.061	0.276	0.432
$E_{\text{MIX-vdW-DF}}$ (eV)	0.004	−0.044	0.125	0.096	0.295	0.459
E_{PBE} (eV)	0.022	−0.366	0.092	...	0.198	0.304

as used for instance in Refs. 60 and 87, and in such cases the width has a well-defined meaning and is given by the value of a specific parameter of the fit function (W in the example given, furthermore A is the maximum value of the reaction probability, and E_0 is the energy at which the reaction probability becomes half its maximum value).

For facilitating a comparison of the energetic corrugation between various functionals, in all cases the early transition state energy on the top site was used, even if the late transition state was higher in energy than the early transition state. Luppi *et al.* previously noted that the PW91 and RPBE functionals showed a large difference in the energetic corrugation.[28] Figure 3, in which the energetic corrugation is plotted against the top to bridge barrier height, shows that the results obtained here support this. A number of features should be pointed out. No very clear overall correlation is found between the lowest barrier height and energetic corrugation of the potential. Functionals with LYP or LDA correlation however show a higher energetic corrugation than the functionals with PBE or Perdew86 correlation, while functionals using vdW-DF or vdW-DF2 correlation show an even

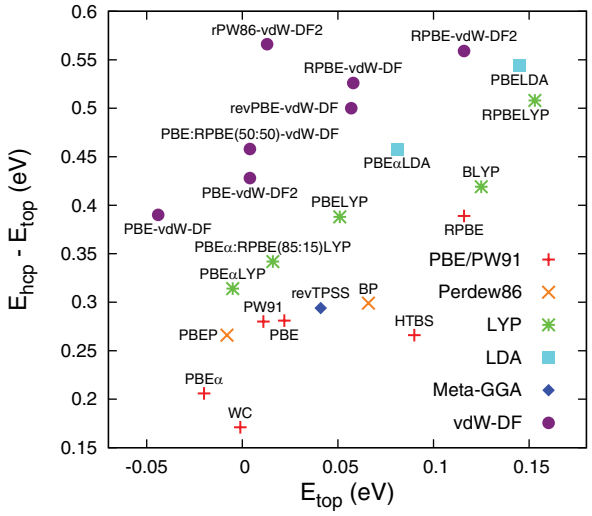

FIG. 3. Energetic corrugation of the potential versus lowest barrier height for the constructed potential energy surfaces. The functionals are grouped (symbols) by correlation functional.

higher energetic corrugation. For the functionals considered here, it seems that the energetic corrugation is higher for the functionals which yield a higher top ($\theta = 90°$, $\phi = 0°$) barrier height. The functionals within a correlation group (i.e., a group of functionals with the same correlation, as indicated in Figure 3 by the use of one specific symbol), show a somewhat stronger correlation between the top ($\theta = 90°$, $\phi = 0°$) barrier height and the energetic corrugation, in the sense that functionals with a higher top to bridge barrier height mostly give a larger energetic corrugation. Such a trend is especially apparent for functionals incorporating a "PBE-like" exchange functional, namely, the exchange functional sequence PBEα → PBE → RPBE, but less so for other exchange functionals such as rPW86 or HTBS. It is not fully understood at present why there is an almost linear correlation between the energetic corrugation and the minimum barrier height for functionals with PBE-like exchange within correlation groups. It is also not completely clear why for H_2 on Ru(0001) the energetic corrugation varies so strongly with the minimum barrier height. It should, however, be pointed out that this could be related to the rather large difference in distance to the surface (Z) of the top($\theta = 90°$, $\phi = 0°$) and hcp($\theta = 90°$, $\phi = 30°$) transition state (also referred to as geometric corrugation[28]): the top($\theta = 90°$, $\phi = 0°$) transition state is much further away from the surface than the hcp($\theta = 90°$, $\phi = 30°$) transition state (see Table VI). For the H_2 on Cu(111) system, the geometric corrugation is smaller (all barriers are late and their positions fall between $Z = 2.2$ and 2.6 bohrs), and for this system no large differences in energetic corrugation between PW91 and RPBE were found, while larger differences were found between PW91 and RPBE barrier heights.[17,18]

In Figure 4, the height of the top to bridge barrier has been plotted against the distance of the same barrier to the surface. There is no clear correlation between the position and height of the barrier. Similar correlations as in Figure 3 can however be found within a correlation group, although these correlations are less clear here. Barriers obtained with vdW-DF functionals are usually closest to the surface, while functionals with PBE or Perdew86 correlation are usually furthest from the surface. The top to bridge barrier can therefore shift about 0.4 Å with the choice of the exchange-correlation functional in Z for a particular top to bridge barrier

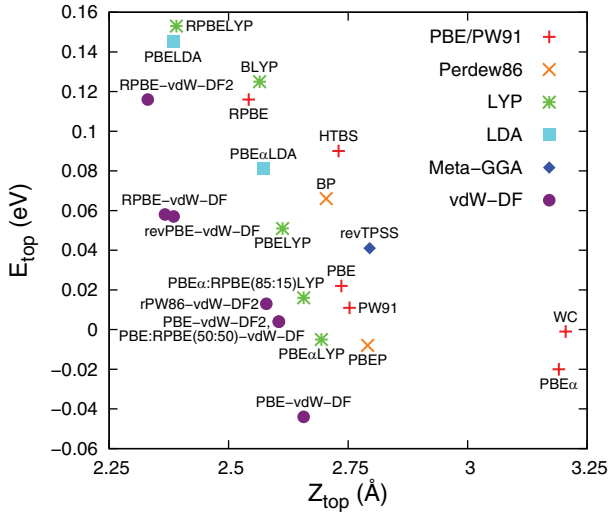

FIG. 4. Height of the top to bridge barrier versus position of the top to bridge barrier for the constructed potential energy surfaces. The functionals are grouped (symbols) by correlation functional.

height. This rather large shift can have dramatic effects on the anisotropy or corrugation of the potential barrier which is experienced by the H_2 molecule. For the functionals considered here, it seems that the barriers are higher the closer they are to the surface, but it should be noted that the correlation is rather weak.

The lattice constants for ruthenium obtained with various functionals were compared to experiment.[76] Because no experimental data are available for low temperatures, also a comparison is made to an extrapolation of experimental data to 0 K.[42] The computed values for the lattice constants are shown in Table IV. It is clear that most functionals overestimate the lattice constant. Of all the functionals which were tested only the revTPSS, WC, and HTBS functionals yield a lattice constant in reasonable agreement with experiment. This is not surprising because the WC functional is a functional created for describing solids,[75] and the HTBS and revTPSS functionals are functionals created to yield a good description of both solids and molecules[67,74] at the GGA and meta-GGA level, respectively.

Finally, in Figure 5 the height of the top to bridge barrier and the energetic corrugation have been plotted against the lattice constant a. There is, as shown in the bottom panel, a rather clear overall correlation between the energetic corrugation and the lattice constant, in the sense that functionals giving a higher energetic corrugation also predict a larger lattice constant. In spite of this clear trend, there is still some variation. In particular, the LYP and LDA functionals considered here, as well as the rPW86-vdW-DF2 functional, yield a relatively low energetic corrugation for the obtained lattice constant. The HTBS and revTPSS functionals yield a relatively high energetic corrugation (similar to the PBE value) for the lattice constants obtained with these functionals. As shown in the top panel of Figure 5, there seems to be no clear overall correlation between the minimum (top to bridge) barrier height and the lattice constant, although a clearer and near-linear correlation is present for functionals containing PBE-

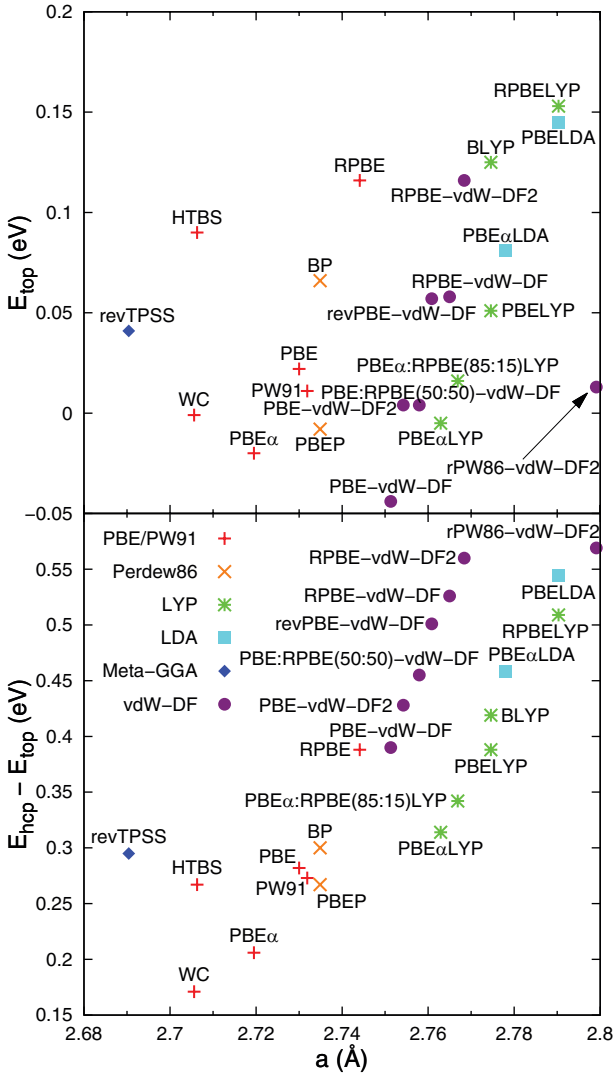

FIG. 5. Height of the top to bridge barrier (top panel) and energetic corrugation (bottom panel) versus lattice constant for the constructed potential energy surfaces. The functionals are grouped (symbols) by correlation functional.

like exchange and belonging to the same correlation group, as in Figures 3 and 4. In fact, this is not so surprising, as a similar correlation has been observed before between the CO adsorption energy on specific metal surfaces and the metal surface energy computed with GGAs[88,89] (interestingly, similar to what is found here, the revTPSS meta-GGA result fell away from the line correlating the CO adsorption energy and the surface energy[89]). A correlation would then be expected also between barrier heights and lattice constants because adsorption energies and reaction barrier heights are correlated (as described by the so-called Brønsted–Evans–Polanyi relations[90,91]), while the metal surface energy and the lattice constant of the metal are both functions of the cohesive strength of the metal.

B. Initial state-resolved reaction and rotational quadrupole alignment

In Figure 6, the initial-state resolved (degeneracy averaged) reaction probability $P_{\mathrm{deg}}(E_i; v, J)$ for H_2 dissociating

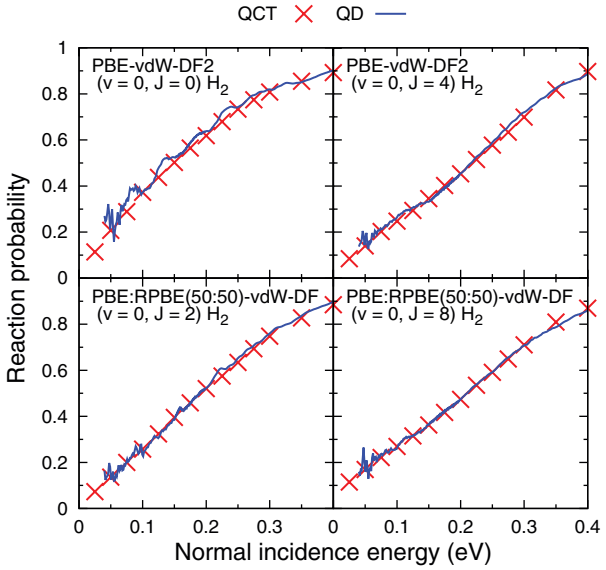

FIG. 6. Comparison between the initial state-resolved reaction probability calculated with quantum dynamics and quasi-classical trajectory calculations.

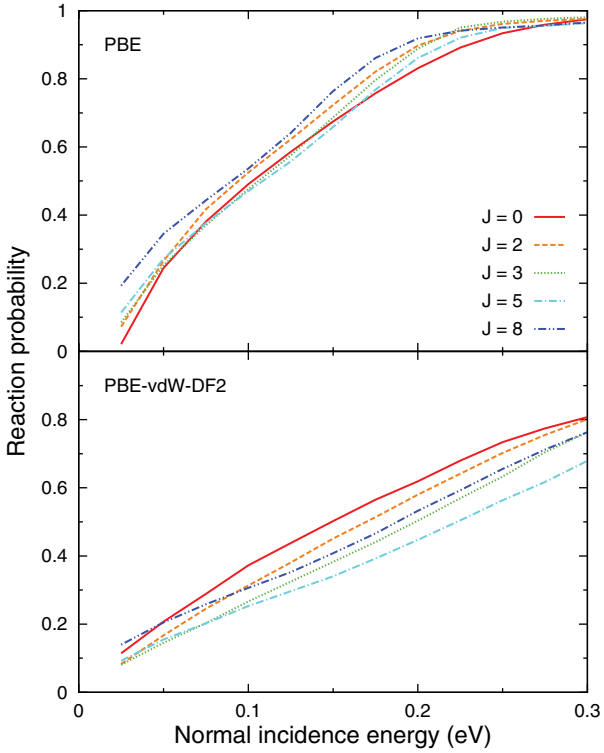

FIG. 7. The degeneracy averaged reaction probability for the PBE and PBE-vdW-DF2 functionals for several rotational states in the vibrational ground state. The probabilities were computed with the quasi-classical trajectory method.

on Ru(0001) obtained from quasi-classical trajectories (QCT) is compared to quantum dynamics (QD) calculations for the PBE-vdW-DF2 and PBE:RPBE(50:50)-vdW-DF functionals. At the lowest energies some small oscillations are present in the QD results. In spite of this, the agreement between QCT and QD is found to be excellent, in particular for the higher rotational states. This good agreement makes it possible to use QCT instead of QD results for the simulation of molecular beams.

In Figure 7, the degeneracy averaged reaction probability for H_2 dissociating on Ru(0001) obtained from QCT is compared for various initial rovibrational states for the PBE and PBE-vdW-DF2 functionals. It is clear that the PBE-vdW-DF2 functional gives rise to less steep reaction probability curves than the PBE functional. This can be understood from the increased energetic corrugation (see Figure 3) of the potential energy surface. Furthermore, the ordering of the curves is different. With the PBE-vdW-DF2 functional first reaction decreases with increasing J up to about $J = 5$, after which reaction increases again with increasing J. With the PBE functional, reaction first slightly increases with J up to $J = 2$, then slightly decreases with J up to $J = 5$, and then increases further with increasing J. This shows that the PBE and PBE-vdW-DF2 functionals clearly have a different anisotropy, as the anisotropy of the potential determines the rotational dependence of reaction. The precise feature of the PES responsible for this difference is however not clear and should be considered beyond the scope of this paper. Because the PBE-vdW-DF2 functional gives barriers which are closer to the surface than the PBE functional however, a larger anisotropy is expected for the PBE-vdW-DF2 functional, which is also found in the potential energy surfaces (see Table VI). The PBE functional gives smaller rotational effects than the PBE-vdW-DF2 functional, consistent with the differences in anisotropy.

It should be noted that for H_2 and D_2 dissociation on Cu(111) experimental studies[60,92,93] showed a behaviour similar to the one here observed with the PBE-vdW-DF2 functional, in the sense that reaction at first decreases with J, after which it increases with J. This trend could not be reproduced in recent calculations[17,18] in which the PW91 and RPBE functionals were used. In these calculations, a behaviour similar to the one here observed with the PBE functional was found. This therefore suggests that the use of vdW-DF functionals on H_2 or D_2 dissociation on Cu(111) could lead to an improved description of that system.

The differences in anisotropy between the PBE and PBE-vdW-DF2 functionals are emphasized even more when the orientational dependence of reaction is considered. In Figure 8, the rotational quadruple alignment parameter computed with QCT is shown for the same two functionals. Several differences are found between the two functionals. The rotational quadrupole alignment parameter for the PBE functional is lower than for the PBE-vdW-DF2 functional. On the investigated interval, the rotational quadrupole alignment parameter reaches a maximum value of about 0.4 for the PBE functional, while the PBE-vdW-DF2 functional reaches a maximum value of about 0.9. This rather large difference can be understood if the positions of the barriers are considered. For example, on the hcp site, the barrier with the PBE functional is at $Z = 1.93$ Å, while the barrier with the PBE-vdW-DF2 functional is at $Z = 1.66$ Å (see also Table VI). This leads to a higher anisotropy on the barrier for the PBE-vdW-DF2 functional, which leads to a higher

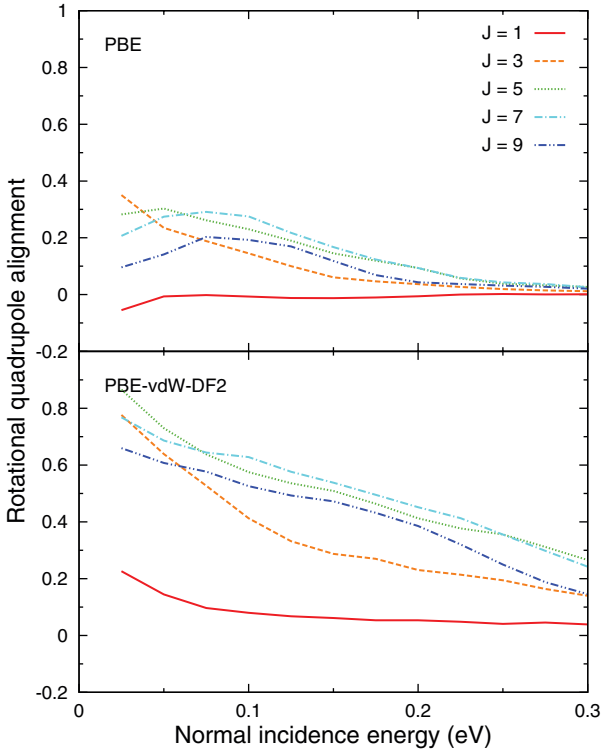

FIG. 8. The rotational quadrupole alignment parameter, computed with the quasi-classical trajectory method, for the PBE and PBE-vdW-DF2 functionals for several rotational states in the vibrational ground state.

rotational quadrupole alignment parameter, because the higher anisotropy leads to an increased preference for reaction of helicoptering molecules.

C. Molecular beam sticking

In Figure 9, the molecular beam simulations for H_2 dissociating on Ru(0001) are shown for several commonly used exchange-correlation functionals. It is clear that, similar to previous results by Nieto *et al*,[30] the computed reaction probability curves are narrower than the experimental curve. For the width, the best agreement is found for the RPBE and BLYP functionals, but both of these underestimate the reaction probability for the lowest collision energies considerably. The potential energy surfaces obtained from these functionals therefore have too high minimum barriers. The PW91 and PBE reaction probability curves are quite similar, which is not surprising as the PBE functional is overall quite similar[68] to PW91. It should be clear that the reaction probability follows the trends shown in Figure 3 for the energetic corrugation and lowest barrier height at least qualitatively.

In Figure 10, the molecular beam simulations for H_2 dissociating on Ru(0001) are shown for the revTPSS and HTBS functionals, with a comparison to results obtained with related functionals. The HTBS functional yields a reaction probability curve which is in between the reaction probability curves obtained with the WC and RPBE functionals. The reaction probability obtained with the HTBS PES at low energies is underestimated, while it is overestimated at high energies. The width of the HTBS reaction probability curve seems to

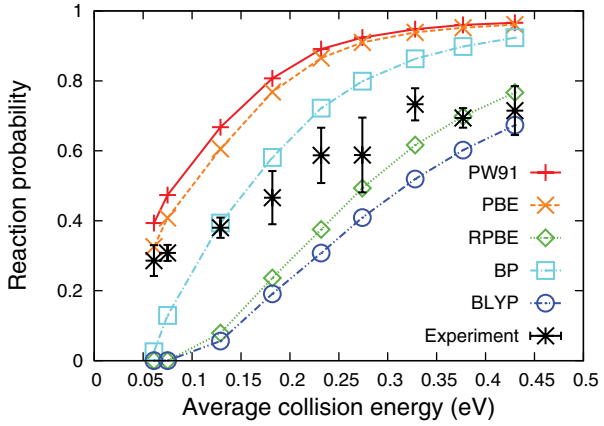

FIG. 9. Reaction probability for molecular beams of H_2 dissociating on Ru(0001) computed with various standard functionals, compared to experiment.[31]

be equal to or even slightly smaller than the width of the PBE reaction probability curve. The revTPSS functional yields reaction probabilities which are slightly lower than PBE and are therefore in better overall agreement with the experiments. The width of the reaction probability curve is however not much changed and can in this sense not explain the experimental dependence of the reaction probability on the incidence energy. It is difficult to say much of general validity about the importance of the meta-GGA approximation for molecule–surface reactions, as only a single meta-GGA functional is tested here for a single system. For the system considered here, however, the strength of the meta-GGA approximation seems to lie in the better simultaneous description of the surface, as evidenced by a better lattice constant (see Table IV), and the molecule–surface interaction, as evidenced by the reaction probabilities computed with the PBE and revTPSS functionals being similar. The better simultaneous description of the molecule and the surface is in agreement with previous results obtained with the revTPSS functional,[89] and is consistent with construction principles used in the development of this functional (better simultaneous description

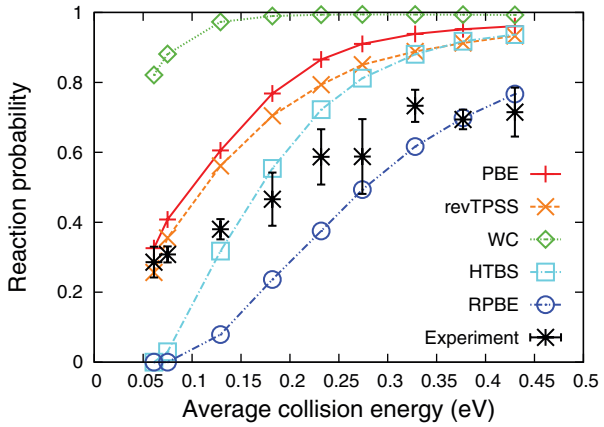

FIG. 10. Reaction probability for molecular beams of H_2 dissociating on Ru(0001) computed with the revTPSS and HTBS functionals. For comparison, the PBE, WC, and RPBE molecular beam reaction probabilities are plotted, as well as experimental results.[31]

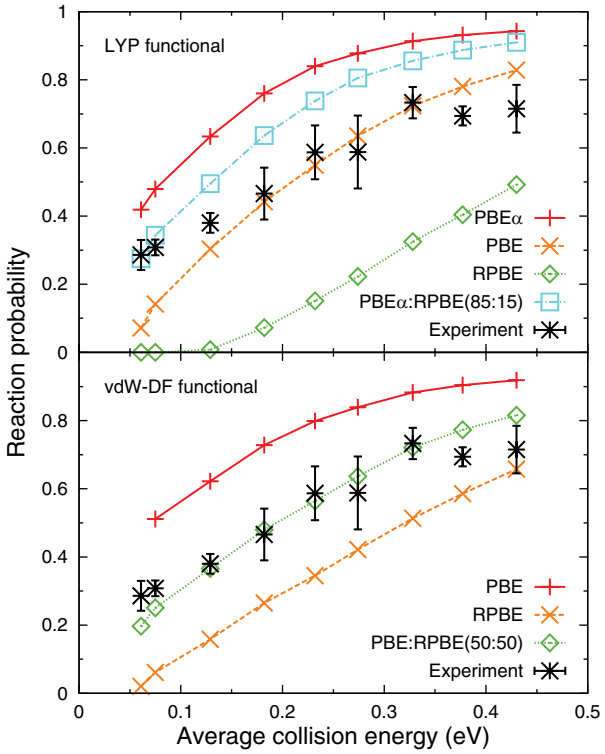

FIG. 11. Reaction probability for molecular beams of H_2 and D_2 dissociating on Ru(0001) computed with various functionals containing LYP and vdW-DF correlation, compared with experimental results.[31] In the legend, only the name of the exchange functional is given.

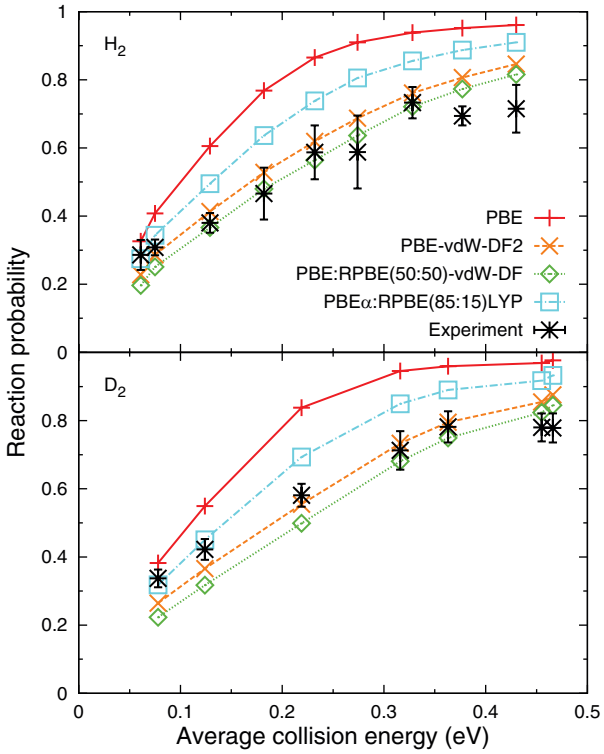

FIG. 12. Reaction probability for molecular beams for H_2 and D_2 dissociating on Ru(0001) computed with the PBE-vdW-DF2 functional and the two mixed functionals of Figure 11, compared with experimental results.[31] For comparison, the PBE molecular beam reaction probability has been plotted.

of molecules and solids).[74] The finding that the revTPSS functional yields similar values of the minimum barrier height and the energetic corrugation for H_2 on Ru(0001) but yield a different and somewhat better value of the Ru lattice constant suggests that meta-GGA functionals could be devised that give a systematically better simultaneous description of surface reactivity and the metal lattice. This could be relevant to being able to simulate reactive scattering processes in a specific system over a large range of surface temperatures.[94]

The relatively high energetic corrugation of the LYP- and vdW-DF-based functionals suggests that if suitable exchange functionals are chosen, they could be used for a mixing procedure similar to the one previously applied for H_2 on Cu(111).[17,18] The results of such a mixing procedure, in which only the exchange functional is mixed and the correlation functional kept fixed, are shown in Figure 11. For the LYP functionals, it is found that PBEαLYP and RPBELYP could form a pair for the mixing procedure, in the sense that one functional consistently overestimates the reaction probability and the other consistently underestimates. The PBE-LYP functional already provides a reasonable description at higher energies, but underestimates the reaction probability at the lowest energies. A 85:15 mixture of the PBEα and RPBE functionals gives a good agreement for the lowest energies. For the vdW-DF functionals, the PBE-vdW-DF and RPBE-vdW-DF functionals could form such a pair. A 50:50 mixture of the PBE and RPBE functionals gives a good agreement over the whole energy range. For the vdW-DF2 functional, it was found that no mixing procedure was needed.

In Figure 12, the molecular beam simulations for H_2 and D_2 dissociating on Ru(0001) are shown for the PBE-vdW-DF2, PBE:RPBE(50:50)-vdW-DF, and PBEα:RPBE(85:15)LYP functionals. The PBE-vdW-DF2 reaction probability is at all points slightly higher than the PBE:RPBE(50:50)-vdW-DF reaction probability, even though the minimum barrier heights are almost the same for these functionals. The PBEα:RPBE(85:15)LYP functional gives a reaction probability curve which is slightly more reactive and narrower. The agreement with experiment is good for both vdW-DF functionals, except perhaps at the highest two energies. It should however be pointed out that a somewhat oscillatory behaviour is present in the experimental data at the highest points, which is not reproduced by theory. Overall, the agreement with experiment is quite good for the two vdW-DF functionals. This suggests that these functionals can be considered candidate SRP functionals.

D. Scattering and reaction at off-normal incidence

In Figure 13, the reaction probability of cold *n*-H_2 (25% $J = 0$, 75% $J = 1$) computed with quantum dynamics is plotted against normal incidence energy for normal and off-normal incidence, for the PBE-vdW-DF2 functional. It should be noted that normal energy scaling does not seem to be completely obeyed. Molecular beam experiments however suggested that normal energy scaling is obeyed.[31] The effect of parallel incidence energy is, at the energies considered, a lowering of the reaction probability, consistent with

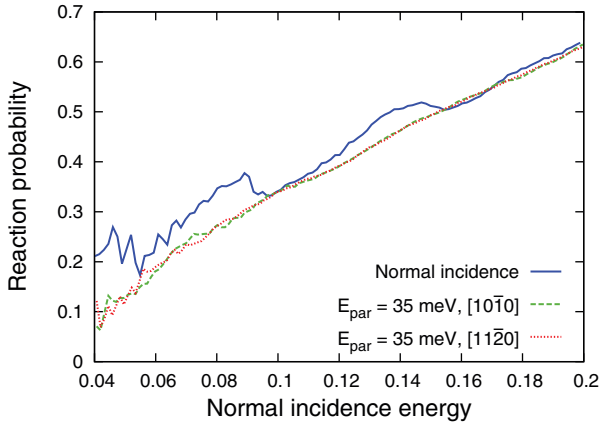

FIG. 13. Reaction probability for n-H_2 reacting on Ru(0001), shown as a function of normal incidence energy, computed with the PBE-vdW-DF2 functional for various incidence conditions.

previous calculations on H_2 dissociation on Pt(111)[45] and model potentials.[95] It should furthermore be noted that small oscillations occur in the curve at low energies, suggesting that the hydrogen molecule can be temporarily trapped in one of the wells present in the PES. These oscillations were not present in previous PW91 results.[30]

In Figure 14, probabilities for various scattering processes computed with quantum dynamics are shown for cold n-H_2 scattering from Ru(0001) with an initial parallel energy of 35 meV in the [11$\bar{2}$0] incidence direction. The reaction probability computed with the PBE-vdW-DF2 and PBE:RPBE(50:50)-vdW-DF functionals is lower than the reaction probability previously obtained with the PW91 functional over the entire range of incidence energies considered. Rotational excitation into $(v' = 0, J' = 2)$ for the vdW-DF functionals has a probability similar to the one previously obtained with the PW91 functional, and is the dominant rovibrational excitation channel. Vibrational excitation is not an open channel at the energies considered here. The probability for survival in $(v' = 0, J' = 0)$ or $(v' = 0, J' = 1)$ is higher with the PBE-vdW-DF2 and PBE:RPBE(50:50)-vdW-DF functionals than those previously obtained with the PW91 functional.

The total per-order diffraction probabilities obtained with the PBE-vdW-DF2 and PBE:RPBE(50:50)-vdW-DF functionals are generally higher than those obtained with PW91. The shape of the per-order diffraction probability curves is however almost the same for the different functionals considered. The second and third order diffraction probabilities do not change much over the considered energy range, while the zeroth and first order diffraction probability curves in all cases decrease with increasing incidence energy. For the vdW-DF based functionals, the total first order diffraction probability is higher than the zeroth order diffraction probability, whereas they are almost the same for the PW91 functional, except at the lowest energies. The PW91 functional is the only functional reproducing the experimental trend that zeroth order diffraction is more probable than first order diffraction, but only at the lowest energies. All functionals predict a reasonable amount of second and third order diffraction, in

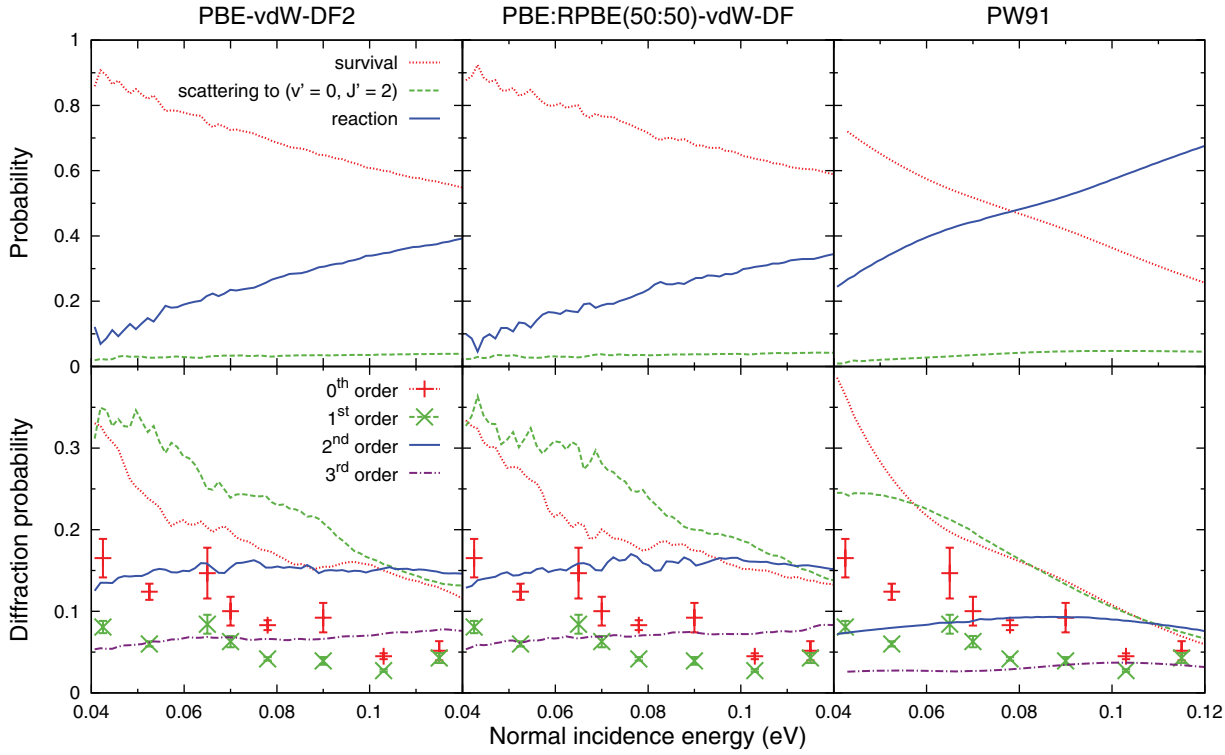

FIG. 14. Various scattering probabilities for n-H_2 scattering from Ru(0001) with an initial parallel energy of 35 meV in the [11$\bar{2}$0] incidence direction computed with the PBE-vdW-DF2 and PBE:RPBE(50:50)-vdW-DF XC functionals. Theoretical results: lines, experimental results:[30] symbols. Top panels: rovibrationally elastic scattering (survival), rotational excitation $(v' = 0, J' = 2)$, and reaction. Bottom panels: per-order diffraction probabilities for rovibrationally elastic scattering. For comparison, previous PW91 results[30] are also shown.

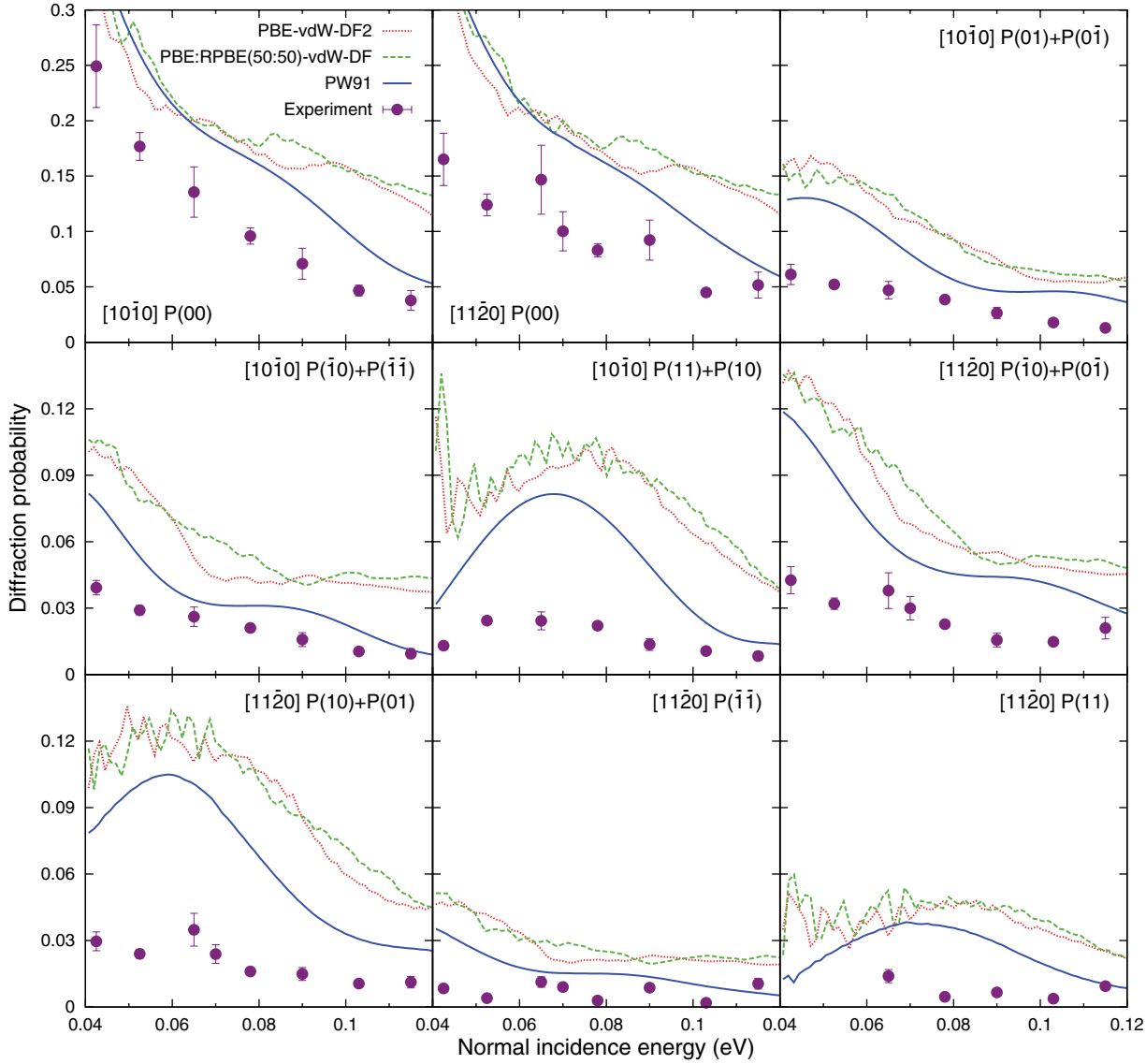

FIG. 15. Diffraction probabilities for n-H_2 scattering from Ru(0001) with an initial parallel energy of 35 meV in the [10$\bar{1}$0] or [11$\bar{2}$0] incidence directions computed with the PBE-vdW-DF2 and PBE:RPBE(50:50)-vdW-DF XC functionals. For comparison, experimental results[30] and previous PW91 results[30] are also shown.

disagreement with experiments (in experiments, second order diffraction channels were found to be an order of magnitude lower in intensity than first order diffraction channels[30]). For the [10$\bar{1}$0] incidence direction similar results were obtained.

In Figure 15, diffraction probabilities for rovibrationally elastic scattering of cold n-H_2 computed with quantum dynamics are shown for the PBE:RPBE(50:50)-vdW-DF and PBE-vdW-DF2 functionals, and compared to experiments and previous results[30] obtained with the PW91 functional. The two vdW-DF functionals considered here, PBE-vdW-DF2 and PBE:RPBE(50:50)-vdW-DF, give results in good agreement with each other. Furthermore, the order of the curves is mostly in agreement with the previous PW91 calculations. The diffraction probability at higher energies is however somewhat higher than obtained with the PW91 calculations, especially at higher incidence energies. The results from the vdW-DF functionals overestimate the experimental diffraction probability by at most about a factor 2 for zeroth order diffraction and by around a factor 3 for first order diffraction.

The agreement with the diffraction experiments is clearly not as good as the agreement obtained for the reaction probability in Sec. III C. The computed diffraction probabilities are too high compared to the experiments, in particular for first order diffraction. There are several possible explanations for this and these will be discussed below.

First, the effects of surface temperature should be considered. For the reaction probability, no large surface temperature effects are expected. This has several reasons. The surface temperature used in the experiments, $T_s = 180$ K,[31] is rather low. In *ab initio* molecular dynamics calculations[39] and static corrugation model calculations,[40] almost no effects were found for H_2 dissociating on Cu(111) at a surface temperature $T_s = 120$ K. While the surface temperature for the molecular beam experiments on H_2 dissociation on Ru(0001) was slightly higher, the experimentalists did not find surface

temperature effects down to $T_s = 140$ K.[31] Furthermore, the lowest barriers in the H_2 on Ru(0001) system are further away from the surface than was the case for H_2 on Cu(111), suggesting a weaker coupling between H_2 and surface degrees of freedom. Finally, energy exchange is not expected to be important for this system due to the large mass mismatch between a H_2 molecule and a ruthenium atom.

The importance of surface temperature effects could however be different for the case of diffraction. In the diffraction experiments, a higher surface temperature of $T_s = 500$ K[30,64] was used. It is known that surface temperature can lead to a dramatic decrease of the measured diffraction probability due to Debye–Waller (DW) attenuation.[96] To correct for this, the experimental data were extrapolated to $T_s = 0$ K using a DW model.[30] Experiments in the range $T_s = 500$–1000 K were found to obey such a DW model.[30] It is, however, not clear to what extent such a model holds below 500 K, as no measurements were possible below this temperature due to a buildup of a hydrogen layer on the surface.[30] The quality of such a DW extrapolation can be tested theoretically by performing calculations at a higher surface temperature. Recently quantum dynamics calculations have been performed for H_2 dissociation on Cu(111) where 1 surface degree has been taken into account either completely (7D) or using a phonon sudden approximation (6+1D).[97] Such calculations, or calculations taking into account even more degrees of freedom, could help clarify to what extent such a DW model holds.

Second, it should be noted that it is not possible to rule out that the exchange-correlation functionals used are still not quite correct, in the sense that they could predict a too weak anisotropy in the PES and therefore a too low rotational excitation probability, and therefore too high rotationally elastic diffraction probabilities. With respect to this possibility, it should be noted that previous calculations using PW91 and RPBE showed a similar rotational excitation probability (at the highest incidence energy considered, approximately 5%[30]), and as such it is not clear whether this could explain the observed discrepancies.

Third, it should be noted that in the theoretical calculations only the ($v = 0$, $J = 0$) and ($v = 0$, $J = 1$) states were considered, while in the experiments also other states than these could be present. It was estimated previously that 73% of the molecules were in the $J = 1$ state at the lowest energy considered in experiments in contrast to 60% at the highest energy considered. As discussed in Sec. III B, the reaction probability decreases slightly with increasing J up to $J = 5$. Assuming normal energy scaling to hold to a reasonable extent, this could lead to an increase of the scattering probabilities of, in the most extreme case ($J = 5$), less than 20% compared to $J = 1$. If all the ortho-H_2 not present in the $J = 1$ state would be in the $J = 5$ state (most would actually be in the $J = 3$ state), this would lead to a change in scattering probability of at most about $20\% \cdot 15\% = 3\%$ at the highest energy considered. A smaller contribution is expected from the para-H_2 molecules. At low energies, the number of rotationally excited molecules is simply too low to come even remotely close to explaining the observed discrepancies. As such, the incorporation of additional rotational states in the calculation is therefore not expected to improve the results considerably.

In summary, it is not yet clear whether the disagreement with the experimental diffraction probabilities reflects a failure of the two candidate SRP density functionals or a failure of the Debye–Waller model to extrapolate the measured diffraction probabilities from $T_s \geq 500$ K to 0 K. Hopefully, future calculations incorporating the effect of surface temperature can resolve this issue. In addition, new and detailed reactive scattering experiments on H_2 + Ru(0001) would be useful, as such experiments could yield observables which can be used to validate the candidate SRP XC functionals, without the incoherent scattering problems that affect diffraction experiments. Examples of such experiments include associative desorption experiments, which by application of detailed balance may yield initial state-resolved reaction probabilities (measured for, for instance, H_2[60] and D_2[93,98] dissociation on Cu(111)). Alternatively, such experiments may also yield rotational state populations (as measured for H_2 + Pd(100)[99]), average translational energies for H_2 desorbing from the surface in particular (v, J) states (as measured for H_2 + Cu(100)[20]) and initial rotational quadrupole alignment parameters describing the orientational dependence of reaction (measured for, for instance, H_2 + Cu(111),[100–102] H_2 + Cu(100),[20] and H_2 + Pd(100)[103]). Additional valuable information can perhaps be obtained from experiments that use laser excitation and detection using resonance enhanced multi-photon ionization (REMPI) to determine probabilities for rotationally inelastic scattering, like the experiments performed earlier for H_2 + Cu(111),[104] H_2,[105] HD,[106] and D_2[107] + Cu(100) and H_2,[108] HD,[106] and D_2[107] + Pd(111).

IV. CONCLUSIONS

Potential energy surfaces have been constructed for the dissociation of H_2 on Ru(0001) from density functional theory calculations, using over 20 different exchange-correlation functionals. To compare with experimentally measured sticking probabilities and diffraction probabilities, quasi-classical and quantum dynamics calculations have been performed.

The functionals investigated yield a wide range of lattice constants, barrier heights, and barrier positions. In particular the energetic corrugation, defined as the difference in barrier height between the hcp and top sites, shows a wide variation. The energetic corrugation is one of the factors determining the width of the reaction probability curve, which was in a previous study found to be too narrow for this system. Functionals containing LYP or LDA correlation yield a higher energetic corrugation than functionals containing PBE or Perdew86 correlation, and functionals containing vdW-DF correlation yield an even higher energetic corrugation. A similar trend was found for the barrier positions, where the vdW-DF functionals yield barriers closest to the surface, and functionals with PBE or Perdew86 correlation yield barriers furthest away from the surface.

From a comparison of the initial state-resolved reaction probability and rotational quadrupole alignment parameter between the PBE functional and the PBE-vdW-DF2 functional, it is concluded that the vdW-DF functional has a higher

anisotropy on the barrier because the barriers obtained with this functional are closer to the surface.

From the comparison to molecular beam sticking experiments, it is concluded that, out of the functionals tested, only functionals which incorporate the van der Waals interaction in an approximate way can reasonably well describe the width of the reaction probability curve, as already expected from the energetic corrugation of these functionals. The PBE-vdW-DF2 and PBE:RPBE(50:50)-vdW-DF functionals describe the sticking experiments reasonably well, with the largest discrepancies occurring at the highest incidence energies, suggesting that these functionals can be considered candidate specific reaction parameter functionals.

For the comparison to diffraction experiments for the PBE-vdW-DF2 and PBE:RPBE(50:50)-vdW-DF functionals, it is found that the computed diffraction probabilities are higher than the Debye–Waller-extrapolated experimental results. Two possible explanations are offered: either the Debye–Waller model cannot be used to extrapolate from the lowest surface temperature probed in experiments ($T_s = 500$ K) to 0 K, or the candidate specific reaction parameter exchange-correlation functionals considerably underestimate the amount of rotational excitation occurring in the scattering process. The first point can be addressed by performing calculations at a higher surface temperature, in which the instantaneous displacements and possibly also motion of surface atoms are taken into account, to test the quality of the Debye–Waller model. Only such calculations can determine whether or not the PBE-vdW-DF2 and PBE:RPBE(50:50)-vdW-DF functionals can also give a good description of diffractive scattering.

ACKNOWLEDGMENTS

The authors would like to thank I. M. N. Groot and L. B. F. Juurlink for useful discussions related to the velocity distributions of the molecular beams used in their experiments, and D. Farías for useful discussions. This research was supported by a TOP grant from Chemical Sciences (CW) of NWO.

[1] W. Kohn and L. J. Sham, Phys. Rev. **140**, A1133 (1965).
[2] P. Hohenberg and W. Kohn, Phys. Rev. **136**, B864 (1964).
[3] D. C. Langreth and M. J. Mehl, Phys. Rev. B **28**, 1809 (1983).
[4] A. D. Becke, Phys. Rev. A **38**, 3098 (1988).
[5] K. Yang, J. Zheng, Y. Zhao, and D. G. Truhlar, J. Chem. Phys. **132**, 164117 (2010).
[6] J. Zheng, Y. Zhao, and D. G. Truhlar, J. Chem. Theory Comput. **5**, 808 (2009).
[7] J. Wellendorff, K. T. Lundgaard, A. Møgelhøj, V. Petzold, D. D. Landis, J. K. Nørskov, T. Bligaard, and K. W. Jacobsen, Phys. Rev. B **85**, 235149 (2012).
[8] J. S. Hummelshøj, F. Abild-Pedersen, F. Studt, T. Bligaard, and J. K. Nørskov, Angew. Chem., Int. Ed. **51**, 272 (2012).
[9] S. Wang, V. Petzold, V. Tripkovic, J. Kleis, J. G. Howalt, E. Skúlason, E. M. Fernández, B. Hvolbæk, G. Jones, A. Toftelund, H. Falsig, M. Björketun, F. Studt, F. Abild-Pedersen, J. Rossmeisl, J. K. Nørskov, and T. Bligaard, Phys. Chem. Chem. Phys. **13**, 20760 (2011).
[10] B. Hammer, L. B. Hansen, and J. K. Nørskov, Phys. Rev. B **59**, 7413 (1999).
[11] G. J. Kroes, Science **321**, 794 (2008).
[12] G. J. Kroes, Phys. Chem. Chem. Phys. **14**, 14966 (2012).
[13] A. Groß, Surf. Sci. Rep. **32**, 291 (1998).
[14] H. F. Busnengo, W. Dong, P. Sautet, and A. Salin, Phys. Rev. Lett. **87**, 127601 (2001).
[15] P. Nieto, E. Pijper, D. Barredo, G. Laurent, R. A. Olsen, E. J. Baerends, G. J. Kroes, and D. Farías, Science **312**, 86 (2006).
[16] J. P. Perdew, J. A. Chevary, S. H. Vosko, K. A. Jackson, M. R. Pederson, D. J. Singh, and C. Fiolhais, Phys. Rev. B **46**, 6671 (1992).
[17] C. Díaz, E. Pijper, R. A. Olsen, H. F. Busnengo, D. J. Auerbach, and G. J. Kroes, Science **326**, 832 (2009).
[18] C. Díaz, R. A. Olsen, D. J. Auerbach, and G. J. Kroes, Phys. Chem. Chem. Phys. **12**, 6499 (2010).
[19] Y. Y. Chuang, M. L. Radhakrishnan, P. L. Fast, C. J. Cramer, and D. G. Truhlar, J. Phys. Chem. A **103**, 4893 (1999).
[20] L. Sementa, M. Wijzenbroek, B. J. van Kolck, M. F. Somers, A. Al-Halabi, H. F. Busnengo, R. A. Olsen, G. J. Kroes, M. Rutkowski, C. Thewes, N. F. Kleimeier, and H. Zacharias, J. Chem. Phys. **138**, 044708 (2013).
[21] S. Dahl, J. Sehested, C. J. H. Jacobsen, E. Törnqvist, and I. Chorkendorff, J. Catal. **192**, 391 (2000).
[22] S. Dahl, P. A. Taylor, E. Törnqvist, and I. Chorkendorff, J. Catal. **178**, 679 (1998).
[23] C. J. H. Jacobsen, S. Dahl, P. L. Hansen, E. Törnqvist, L. Jensen, H. Topsøe, D. V. Prip, P. B. Møenshaug, and I. Chorkendorff, J. Mol. Catal. A: Chem. **163**, 19 (2000).
[24] S. Uchiyama, Y. Hattori, K. Aika, and A. Ozaki, Chem. Lett. **10**, 1463 (1981).
[25] K. Honkala, A. Hellman, I. N. Remediakis, A. Logadottir, A. Carlsson, S. Dahl, C. H. Christensen, and J. K. Nørskov, Science **307**, 555 (2005).
[26] L. R. Danielson, M. J. Dresser, E. E. Donaldson, and J. T. Dickinson, Surf. Sci. **71**, 599 (1978).
[27] T. Matsushima, Surf. Sci. **197**, L287 (1988).
[28] M. Luppi, R. A. Olsen, and E. J. Baerends, Phys. Chem. Chem. Phys. **8**, 688 (2006).
[29] J. K. Vincent, R. A. Olsen, G. J. Kroes, M. Luppi, and E. J. Baerends, J. Chem. Phys. **122**, 044701 (2005).
[30] P. Nieto, D. Farías, R. Miranda, M. Luppi, E. J. Baerends, M. F. Somers, M. J. T. C. van der Niet, R. A. Olsen, and G. J. Kroes, Phys. Chem. Chem. Phys. **13**, 8583 (2011).
[31] I. M. N. Groot, H. Ueta, M. J. T. C. van der Niet, A. W. Kleyn, and L. B. F. Juurlink, J. Chem. Phys. **127**, 244701 (2007).
[32] F. O. Kannemann and A. D. Becke, J. Chem. Theory Comput. **5**, 719 (2009).
[33] J. Klimeš and A. Michaelides, J. Chem. Phys. **137**, 120901 (2012).
[34] G. Füchsel, S. Schimka, and P. Saalfrank, J. Phys. Chem. A **117**, 8761 (2013).
[35] M. Born and R. Oppenheimer, Ann. Phys. **389**, 457 (1927).
[36] A. C. Luntz and M. Persson, J. Chem. Phys. **123**, 074704 (2005).
[37] A. S. Muzas, J. I. Juaristi, M. Alducin, R. Díez Muiño, G. J. Kroes, and C. Díaz, J. Chem. Phys. **137**, 064707 (2012).
[38] J. I. Juaristi, M. Alducin, R. Díez Muiño, H. F. Busnengo, and A. Salin, Phys. Rev. Lett. **100**, 116102 (2008).
[39] F. Nattino, C. Díaz, B. Jackson, and G. J. Kroes, Phys. Rev. Lett. **108**, 236104 (2012).
[40] M. Wijzenbroek and M. F. Somers, J. Chem. Phys. **137**, 054703 (2012).
[41] A. Mondal, M. Wijzenbroek, M. Bonfanti, C. Díaz, and G. J. Kroes, J. Phys. Chem. A **117**, 8770 (2013).
[42] J. W. Arblaster, Platinum Met. Rev. **56**, 181 (2012).
[43] A. P. Baddorf, V. Jahns, D. M. Zehner, H. Zajonz, and D. Gibbs, Surf. Sci. **498**, 74 (2002).
[44] R. Kosloff, J. Phys. Chem. **92**, 2087 (1988).
[45] E. Pijper, G. J. Kroes, R. A. Olsen, and E. J. Baerends, J. Chem. Phys. **117**, 5885 (2002).
[46] J. C. Light, I. P. Hamilton, and J. V. Lill, J. Chem. Phys. **82**, 1400 (1985).
[47] G. C. Corey and D. Lemoine, J. Chem. Phys. **97**, 4115 (1992).
[48] D. Lemoine, J. Chem. Phys. **101**, 10526 (1994).
[49] D. Kosloff and R. Kosloff, J. Comput. Phys. **52**, 35 (1983).
[50] M. D. Feit, J. A. Fleck, Jr., and A. Steiger, J. Comput. Phys. **47**, 412 (1982).
[51] G. G. Balint-Kurti, R. N. Dixon, and C. C. Marston, J. Chem. Soc., Faraday Trans. **86**, 1741 (1990).
[52] G. G. Balint-Kurti, R. N. Dixon, and C. C. Marston, Int. Rev. Phys. Chem. **11**, 317 (1992).
[53] R. C. Mowrey and G. J. Kroes, J. Chem. Phys. **103**, 1216 (1995).
[54] A. Vibók and G. G. Balint-Kurti, J. Phys. Chem. **96**, 8712 (1992).
[55] M. Karplus, R. N. Porter, and R. D. Sharma, J. Chem. Phys. **43**, 3259 (1965).

[56]J. Stoer and R. Bulirsch, *Introduction to Numerical Analysis* (Springer, New York, 1980).
[57]H. F. Busnengo, A. Salin, and W. Dong, J. Chem. Phys. **112**, 7641 (2000).
[58]R. A. Olsen, H. F. Busnengo, A. Salin, M. F. Somers, G. J. Kroes, and E. J. Baerends, J. Chem. Phys. **116**, 3841 (2002).
[59]R. N. Zare, *Angular Momentum* (Wiley, New York, 1988).
[60]C. T. Rettner, H. A. Michelsen, and D. J. Auerbach, J. Chem. Phys. **102**, 4625 (1995).
[61]H. A. Michelsen and D. J. Auerbach, J. Chem. Phys. **94**, 7502 (1991).
[62]D. J. Auerbach, in *Atomic and Molecular Beam Methods*, edited by G. Scoles (Oxford University Press, Oxford, 1988), Vol. 1, Chap. 14.
[63]I. M. N. Groot, personal communication (2013).
[64]P. Nieto, D. Barredo, D. Farías, and R. Miranda, J. Phys. Chem. A **115**, 7283 (2011).
[65]C. Lee, W. Yang, and R. G. Parr, Phys. Rev. B **37**, 785 (1988).
[66]J. P. Perdew, Phys. Rev. B **33**, 8822 (1986).
[67]P. Haas, F. Tran, P. Blaha, and K. Schwarz, Phys. Rev. B **83**, 205117 (2011).
[68]J. P. Perdew, K. Burke, and M. Ernzerhof, Phys. Rev. Lett. **77**, 3865 (1996).
[69]G. K. H. Madsen, Phys. Rev. B **75**, 195108 (2007).
[70]J. P. Perdew and Y. Wang, Phys. Rev. B **45**, 13244 (1992).
[71]M. Dion, H. Rydberg, E. Schröder, D. C. Langreth, and B. I. Lundqvist, Phys. Rev. Lett. **92**, 246401 (2004).
[72]K. Lee, E. D. Murray, L. Kong, B. I. Lundqvist, and D. C. Langreth, Phys. Rev. B **82**, 081101 (2010).
[73]Y. Zhang and W. Yang, Phys. Rev. Lett. **80**, 890 (1998).
[74]J. P. Perdew, A. Ruzsinszky, G. I. Csonka, L. A. Constantin, and J. Sun, Phys. Rev. Lett. **103**, 026403 (2009).
[75]Z. Wu and R. E. Cohen, Phys. Rev. B **73**, 235116 (2006).
[76]M. Černohorský, Acta Crystallogr. **13**, 823 (1960).
[77]G. Kresse and J. Hafner, Phys. Rev. B **47**, 558 (1993).
[78]G. Kresse and J. Furthmüller, Comput. Mater. Sci. **6**, 15 (1996).
[79]G. Kresse and J. Furthmüller, Phys. Rev. B **54**, 11169 (1996).
[80]M. A. L. Marques, M. J. T. Oliveira, and T. Burnus, Comput. Phys. Commun. **183**, 2272 (2012).
[81]G. Kresse and J. Hafner, J. Phys.: Condens. Matter **6**, 8245 (1994).
[82]D. Vanderbilt, Phys. Rev. B **41**, 7892 (1990).
[83]P. E. Blöchl, Phys. Rev. B **50**, 17953 (1994).
[84]G. Kresse and D. Joubert, Phys. Rev. B **59**, 1758 (1999).
[85]G. Román-Pérez and J. M. Soler, Phys. Rev. Lett. **103**, 096102 (2009).
[86]A. Groß, B. Hammer, M. Scheffler, and W. Brenig, Phys. Rev. Lett. **73**, 3121 (1994).
[87]H. A. Michelsen, C. T. Rettner, and D. J. Auerbach, Surf. Sci. **272**, 65 (1992).
[88]L. Schimka, J. Harl, A. Stroppa, A. Grüneis, M. Marsman, F. Mittendorfer, and G. Kresse, Nat. Mater. **9**, 741 (2010).
[89]J. Sun, M. Marsman, A. Ruzsinszky, G. Kresse, and J. P. Perdew, Phys. Rev. B **83**, 121410(R) (2011).
[90]J. K. Nørskov, T. Bligaard, A. Logadottir, S. Bahn, L. B. Hansen, M. Bollinger, H. Bengaard, B. Hammer, Z. Sljivancanin, M. Mavrikakis, Y. Xu, S. Dahl, and C. J. H. Jacobsen, J. Catal. **209**, 275 (2002).
[91]J. K. Nørskov, F. Abild-Pedersen, F. Studt, and T. Bligaard, Proc. Natl. Acad. Sci. U.S.A. **108**, 937 (2011).
[92]H. A. Michelsen, C. T. Rettner, and D. J. Auerbach, Phys. Rev. Lett. **69**, 2678 (1992).
[93]H. A. Michelsen, C. T. Rettner, D. J. Auerbach, and R. N. Zare, J. Chem. Phys. **98**, 8294 (1993).
[94]A. A. Marashdeh, S. Casolo, L. Sementa, H. Zacharias, and G. J. Kroes, J. Phys. Chem. C **117**, 8851 (2013).
[95]G. R. Darling and S. Holloway, Surf. Sci. **304**, L461 (1994).
[96]D. Farías and R. Miranda, Prog. Surf. Sci. **86**, 222 (2011).
[97]M. Bonfanti, M. F. Somers, C. Díaz, H. F. Busnengo, and G. J. Kroes, Z. Phys. Chem. **227**, 1397 (2013).
[98]C. T. Rettner, D. J. Auerbach, and H. A. Michelsen, Phys. Rev. Lett. **68**, 1164 (1992).
[99]D. Wetzig, M. Rutkowski, H. Zacharias, and A. Groß, Phys. Rev. B **63**, 205412 (2001).
[100]H. Hou, S. J. Gulding, C. T. Rettner, A. M. Wodtke, and D. J. Auerbach, Science **277**, 80 (1997).
[101]D. Wetzig, M. Rutkowski, R. David, and H. Zacharias, Europhys. Lett. **36**, 31 (1996).
[102]S. J. Gulding, A. M. Wodtke, H. Hou, C. T. Rettner, H. A. Michelsen, and D. J. Auerbach, J. Chem. Phys. **105**, 9702 (1996).
[103]D. Wetzig, R. Dopheide, M. Rutkowski, R. David, and H. Zacharias, Phys. Rev. Lett. **76**, 463 (1996).
[104]A. Hodgson, P. Samson, A. Wight, and C. Cottrell, Phys. Rev. Lett. **78**, 963 (1997).
[105]E. Watts and G. O. Sitz, J. Chem. Phys. **114**, 4171 (2001).
[106]L. C. Shackman and G. O. Sitz, J. Chem. Phys. **122**, 114702 (2005).
[107]L. C. Shackman and G. O. Sitz, J. Chem. Phys. **123**, 064712 (2005).
[108]M. Gostein, E. Watts, and G. O. Sitz, Phys. Rev. Lett. **79**, 2891 (1997).